Volume 6
Number 13
7 July 2025
Pages 4147–4552

Materials Advances

rsc.li/materials-advances

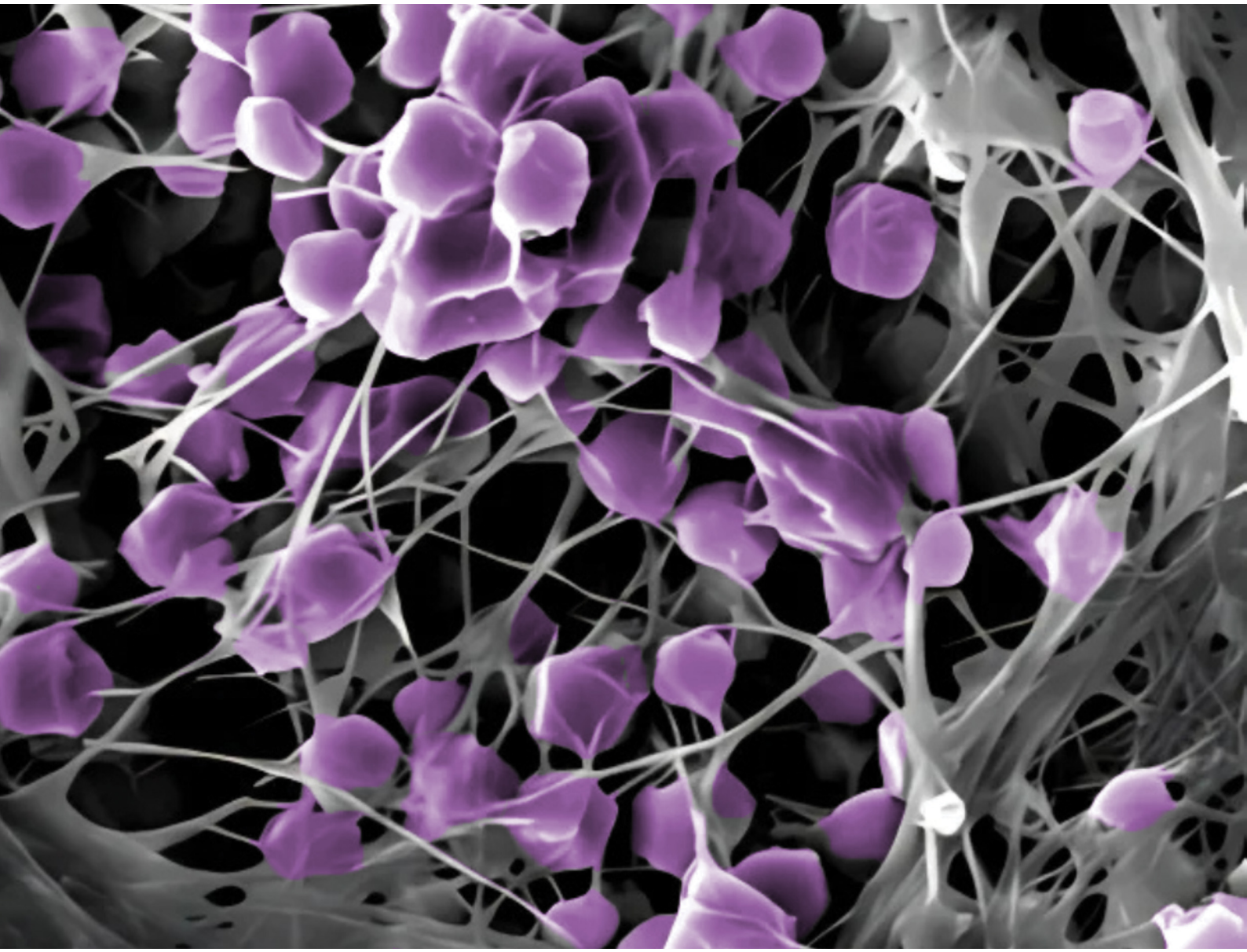

ISSN 2633-5409

ROYAL SOCIETY OF CHEMISTRY

PAPER

Koon-Yang Lee *et al.*

Zeolitic imidazolate framework decorated bacterial cellulose coating for enhancing particulate filtration and adsorption from liquid and vapour phases of woven fabric

Materials Advances

ROYAL SOCIETY OF CHEMISTRY

PAPER

View Article Online
View Journal | View Issue

Cite this: *Mater. Adv.*, 2025, 6, 4202

Zeolitic imidazolate framework decorated bacterial cellulose coating for enhancing particulate filtration and adsorption from liquid and vapour phases of woven fabric†

Joanne Li,[a] Armando Garcia,[b] Anett Kondor,[b] Corinne Stone,[c] Martin Smith,[c] Mike Dennis[c] and Koon-Yang Lee *[ad]

There is currently a timely need for protective textiles used against hazardous chemical warfare agents (CWAs) to move away from fluorinated polymers due to the increasing environmental and health concerns associated with perfluoroalkyl substances. This represents a technical challenge as fluorinated surfaces are important to impart hydrophobicity and oleophobicity to prevent liquid CWAs from reaching the skin level. In this work, we report an alternative approach to increase the adsorption capacity and barrier properties of textiles through metal–organic framework decorated nanocellulose. Bacterial cellulose (BC) was decorated with zeolitic imidazolate framework (ZIF-67) through the growing of ZIF-67 in the presence of BC. ZIF-BC possessed a higher surface area of ~400 m^2 g^{-1}, higher *n*-hexane and ethanol vapour sorption, as well as higher Congo red liquid sorption capacities compared to neat BC. When used as an ultra-low grammage coating for an open porous woven textile substrate, ZIF-67 decorated BC was able to offer an enhanced barrier performance in terms of reduced air permeability and increased aerosol particulate filtration efficiency (up to 97% for PM_1 at a coating grammage of 1 g m^{-2}) without sacrificing moisture transmission rate compared to uncoated woven textile and woven textile decorated with ZIF-67 only. Our work opens up new possibilities in the fluorine-free coating of protective textiles.

Received 17th January 2025,
Accepted 30th April 2025

DOI: 10.1039/d5ma00048c

rsc.li/materials-advances

Introduction

Chemical warfare agents (CWAs) pose great threats to military personnel. A high level of protection is thus imperative to minimise or eliminate the exposure to these hazards especially during combative scenarios. Current permeable protective suits feature an outer shell layer functionalised with a fluorinated polymer to repel liquid CWAs before they reach the inner activated carbon lining. Despite the importance of this liquid repellency, precursors to fluorinated polymers, such as perfluoroalkyl carboxylic acids and perfluoroalkane sulfonic acids have been banned under the persistent organic pollutants regulations in the Stockholm Convention.[1] There is therefore a timely need to develop fluorine-free approaches to continuously protect military personnel from the risks arising from liquid CWAs.

One alternative approach to prevent liquid CWAs from penetrating the protective suit is to increase the adsorption capacity of the shell layer. In this context, metal–organic frameworks (MOFs) are ideal candidates. Due to their tuneable pore size and shape, active functionalities and high surface area, MOFs are currently being explored for a plethora of applications in adsorption, catalysis and drug delivery.[2,3] Among the various families of MOFs, zeolitic imidazolate frameworks (ZIFs) are of particular interest as they are stable in water[4] and can be synthesised at atmospheric pressure and room temperature,[5] which reduce their barrier towards large-scale production.

ZIFs are commonly decorated onto a substrate or a support and are seldomly used in the form of bulk powder or colloidal crystals.[6–8] For instance, ZIF-67 had been anchored onto cellulose aerogels for dye and organic pollutants removal.[9] A high weight loading of ZIF-67 (~40%) could be achieved, particularly when ZIF-67 was grown directly onto the cellulose aerogel. This also increased the specific surface area of the resulting ZIF-67 decorated cellulose aerogels from ~30 m^2 g^{-1} to ~1600 m^2 g^{-1}.

[a] Department of Aeronautics, Imperial College London, South Kensington Campus, London, SW7 2AZ, UK. E-mail: koonyang.lee@imperial.ac.uk
[b] Surface Measurement Systems Ltd, Allentown, PA 18103, USA
[c] Defence Science and Technology Laboratory (dstl), Porton Down, Salisbury, Wiltshire, SP4 0JQ, UK
[d] Institute for Molecular Science and Engineering (IMSE), Imperial College London, South Kensington Campus, London, SW7 2AZ, UK

† Electronic supplementary information (ESI) available. See DOI: https://doi.org/10.1039/d5ma00048c

A degradation rate of organic pollutants by up to 80% was attained within 20 min with the ZIF-67 decorated cellulose aerogel across a wide range of pH.[10] By comparison, neat cellulose aerogel could only degrade up to 10%. Similarly, the adsorption capacity towards methyl orange dye also doubled over neat cellulose aerogel, reaching 134 mg g^{-1} with ZIF-67 decoration onto cellulose aerogels.[11] Besides, ZIF-67 had also been combined with nanocellulose for adsorption applications. Mai *et al.*[12] prepared ZIF-67 and bacterial nanocellulose composite films *via in situ* anchoring for dye removal. At a ZIF loading of 97.3%, the BET surface area of the composite films increased by 85 times to 67 m^2 g^{-1} when compared to that of neat bacterial cellulose and a dye removal efficiency of 98.7% was achieved. TEMPO-oxidised nanocellulose aerogels functionalised with ZIF-67 were also reported for dye adsorption applications.[13,14] With a ZIF-67 loading of ~70%, the nanocellulose/ZIF-67 aerogels exhibited enhanced dye adsorption capacity of up to 60 mg g^{-1}, 3 times higher than that of neat nanocellulose aerogels.

Despite the high adsorption capacity, using ZIF-67/nanocellulose as a monolithic construct (*e.g.*, porous aerogel and self-standing membranes) is unfavourable given its high cost. With an estimated nanocellulose price of at least USD100 per kg (wet basis, 99% moisture content),[15] the enhancement in adsorption performance will be outweighed by the extremely high material cost. We have previously shown that the coating of ultra-low grammage microbially-synthesised nanocellulose, more commonly known as bacterial cellulose or BC, onto a plain weave cotton fabric can increase its aerosol particulate filtration performance without sacrificing its water vapour transmission rate.[16] This is essential to the design of protective suit as maintaining moisture permeability prevents high thermal strain and ensures the physiological comfort of the user.[17] Herein, we built upon our previous innovation on such ultra-low grammage coating layer and report the application of ZIF-67 decorated BC for contaminants removal. It is anticipated that the high cost of nanocellulose can be offset by the ultra-low grammage of nanocellulose used in the coating layer. The ZIF-67 decoration would enhance the adsorption of contaminant molecules while the BC acts as a physical barrier to the aerosolised particulates, making the ZIF-67 decorated BC a multifunctional coating for the shell layer of a chemical and biological protective suit.

Experiments

Materials

Woven cotton fabric (plain weave, mesh aperture = 70 μm, yarn diameter = 0.23 mm, areal density = 150 g m^{-2}) was purchased from Dalston Mill Fabrics (London, UK). Sodium hydroxide pellets (Reag. Ph. Eur., purity > 99%), methanol (AnalaR NORMAPUR, purity = 100%), *n*-hexane (GPR RECTAPUR, purity > 99.9%) and ethanol (AnalaR NORMAPUR, purity = 100%) were purchased from VWR International Ltd (Lutterworth, UK). Cobalt(II) nitrate hexahydrate ($Co(NO_3)_2{\cdot}H_2O$) (purity > 98%), 2-methylimidazole (2-MIM) (purity > 99%), ammonium nitrate (BioXtra, purity > 99.5%) and Congo red were purchased from Sigma Aldrich (Dorset, UK). These chemicals were used as received without further purification. BC in a form of 30 cm × 25 cm × 1 cm pellicle with a water content of 99 wt% was purchased from a commercial retailer (Vietcoco International Co. Ltd, Ho Chi Minh City, Vietnam). It was purified with 0.1 M sodium hydroxide in house following a previously described protocol[18] and stored in a 4 °C fridge prior to subsequent use. In some experiments, freeze-dried BC and ZIF-BC, produced by freezing a suspension of (ZIF-)BC-in-water (*ca.* 1% consistency) at −15 °C followed by freeze drying (Alpha 1-2 LDplus, Martin Christ, Germany), were used.

Synthesis of ZIF-67 and ZIF-67 decorated BC

ZIF-67 was synthesised following a previously described protocol (Fig. 1a).[5,19] Briefly, a solution of $Co(NO_3)_2{\cdot}6H_2O$ (0.9 g) in methanol (50 mL) and a solution of 2-MIM (1 g) in methanol (50 mL) were first prepared. These two solutions were then mixed for 12 h under magnetic stirring at room temperature. After which, the ZIF-67 precipitates were collected by centrifugation (Sigma 4-16S, Sigma Aldrich, Dorset, UK) at 8000 rpm for 10 min and repeatedly washed with methanol (3 × 250 mL) prior to drying at 120 °C for another 12 h. To decorate BC with ZIF-67 (Fig. 1b), the purified BC pellicle (0.1 g, dry basis) was first blended in deionised water at a consistency of 1 wt% using a kitchen blender (Optimum 9400, Froothie Ltd, Cranleigh, UK) operating at a maximum power output of 1000 W for 3 min. The BC-in-water suspension was then solvent exchanged into methanol (3 × 250 mL) through centrifugation (8000 rpm, 20 min). After the last centrifugation step, the BC-in-methanol gel (*ca.* 3% consistency) was then dispersed in 50 mL of methanol with $Co(NO_3)_2{\cdot}6H_2O$ (0.9 g) dissolved. This mixture was stirred for 4 h to disperse the BC-in-methanol gel prior to the addition of

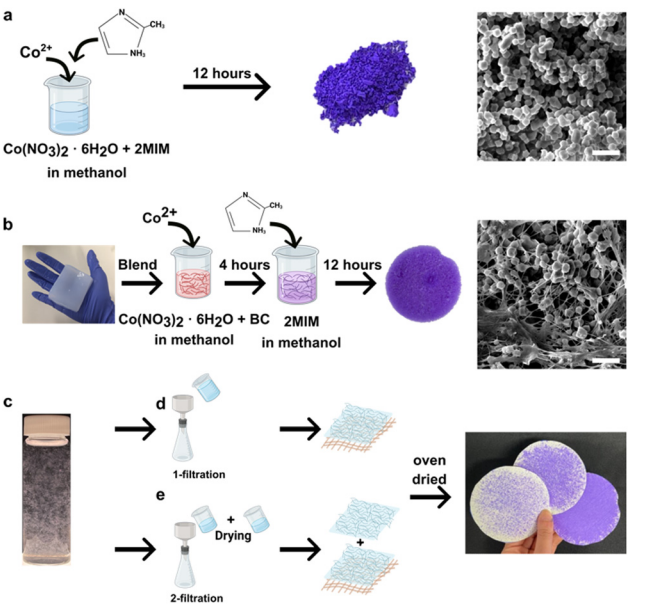

Fig. 1 Schematic diagram summarising the (a) synthesis of ZIF-67, (b) synthesis of ZIF-BC, as well as (c) ZIF-BC coated woven fabric, whereby a suspension of ZIF-BC in water was coated using either the (d) "1-filtration strategy" or (e) "2-filtration strategy" to produce the final product.

0.25 M 2-MIM in methanol solution (50 mL). The resulting mixture was further magnetically stirred for another 12 h at room temperature. After which, the ZIF-67 decorated BC, herein termed ZIF-BC, was collected by centrifugation (8000 rpm, 20 min) and repeatedly washed with methanol (3 × 250 mL) to remove any unattached ZIF-67 particles, as well as any unreacted reactants. Finally, the ZIF-BC was solvent exchanged into deionised water (3 × 250 mL) and stored in a 4 °C fridge prior to subsequent use.

Preparation of woven fabric with ultra-low grammage ZIF-BC coating

The coating of ZIF-BC onto a plain weave woven cotton fabric (Fig. 1c) was adapted from a previous work.[16] Briefly, a ZIF-BC in water suspension (100 mL) was first created using a kitchen blender operating at a maximum power output of 1000 W for 3 min. The prepared ZIF-BC in water suspension was then vacuum filtered onto a 115 mm diameter woven fabric in a Büchner funnel. Two different filtration strategies were employed. In the single filtration strategy (herein termed "1-filtration", see Fig. 1d), the full 100 mL of ZIF-BC in water suspension was vacuum filtered onto the woven fabric in a single step. The resulting ZIF-BC coated woven fabric was then dried in an oven at 120 °C for 30 min under restrain to prevent shrinkage. In the double filtration strategy (herein termed "2-filtration", see Fig. 1e), 50 mL of the ZIF-BC in water suspension was first vacuum filtered onto the woven fabric, followed by drying as aforementioned prior to vacuum filtering the remaining 50 mL of ZIF-BC in water suspension, followed by another drying step. Woven fabric with three different BC grammages were produced in this work, namely 0.25 g m^{-2}, 0.5 g m^{-2} and 1 g m^{-2}, respectively.

Scanning electron microscopy (SEM)

SEM (Tescan Mira, Cambridge, UK) was used to characterise the morphology of the samples. An accelerating voltage of 1 kV and a beam current of 300 pA were used. Prior to SEM, all samples were mounted onto aluminium SEM stubs using carbon tabs and sputter coated with Cr (Q150T ES, Quorum, East Sussex, UK) using a coating current of 120 mA for 210 s.

X-ray diffraction (XRD)

X-ray diffraction (XRD) patterns of freeze dried BC, ZIF-67 and freeze-dried ZIF-BC were obtained using a powder X-ray diffractometer (PANalytical X'pert Pro, PANalytical Ltd, Cambridge, UK) equipped with a 1.54 Å Cu Kα X-ray source. Measurements were taken between $2\theta = 5^\circ$ and 40° using a step size of 0.05° and a scan speed of 0.1° s^{-1}. The simulated XRD pattern of ZIF-67 was retrieved from the Crystallography Open Database.

Attenuated total reflection – Fourier transform infrared (ATR-FTIR) spectroscopy

ATR-FTIR spectra of freeze-dried BC, ZIF-67 and freeze-dried ZIF-BC were obtained using Spectrum One FTIR spectrometer (PerkinElmer, Buckinghamshire, UK). The spectra were collected between 650 and 4000 cm^{-1}. The resolution of the spectra was 0.5 cm^{-1} and a total of 128 scans were performed to obtain each spectrum.

Amount of ZIF-67 decorated on BC

The weight fraction of ZIF-67 ($w_{ZIF\text{-}67}$) decorated onto BC was determined gravimetrically using thermal gravimetric analysis (TGA) (Discovery TGA, TA Instruments, Elstree, UK). Approximate 5 mg of sample was heated from 30 °C to 700 °C at a rate of 10 °C min^{-1} in a N_2 atmosphere. The loading of ZIF-67 on ZIF-BC was determined from the residual weight fraction (x) of the samples at 700 °C using:

$$w_{ZIF\text{-}67}\ (\%) = (x_{ZIF\text{-}BC} - x_{BC})/(x_{ZIF\text{-}67} - x_{BC}).$$

Specific surface area of freeze-dried BC, ZIF-67 and freeze-dried ZIF-BC

The specific surface area of these samples was measured using volumetric N_2 adsorption/desorption at −196 °C (TriStar II 3020, Micrometrics Ltd, Gloucestershire, UK). A sample mass of *ca.* 20 mg was used. Prior to this measurement, the samples were degassed (Flow prep 06, Micrometrics, Gloucestershire, UK) at 80 °C for 12 h under continuous dry N_2 flow to remove any adsorbed water molecules.

Dynamic *n*-hexane and ethanol vapour sorption of freeze-dried BC, ZIF-67 and freeze-dried ZIF-BC

The vapour adsorption isotherms of *n*-hexane and ethanol were evaluated gravimetrically using dynamic vapour sorption (DVS Resolution, Surface Measurement Systems Ltd, Alperton, UK) with compressed air as the carrier gas. Approximately 20 mg of sample was placed in the sample chamber and pre-conditioned *in situ* at 120 °C for 3 h under continuous dry N_2 flow. The sample was then equilibrated at 0% partial pressure (P/P_0) at 25 °C, followed by an increase at a 1% step between $0\% < P/P_0 \leq 20\%$ and a 5% step between $20\% < P/P_0 \leq 90\%$. A fixed rate of mass change (dm/dt) value of 0.001% min^{-1} was selected, with a minimum stage time of 10 min.

Congo red adsorption of freeze-dried BC, freeze-dried ZIF-BC, as well as the (coated) woven fabric

Aqueous Congo red solutions with initial concentration (C_0) ranging between 5 and 50 mg L^{-1} were first prepared. The pH of the solutions was *ca.* 8.2. For each Congo red adsorption experiment, approximately 5–20 mg of sample was placed in 50 mL of aqueous Congo red solution for 24 h at room temperature. After which, the equilibrium Congo red concentration in the solution (C_e, mg L^{-1}) was analysed using UV/vis (Lambda 356, PerkinElmer LAS Ltd, Beaconsfield, UK) at 498 nm. The scanning speed used in this UV/vis measurement was 240 nm min^{-1} and the wavelength range collected was 400–700 nm. The amount of Congo red adsorbed by the sample at equilibrium (q_e, mg g^{-1}) was calculated from: $q_e = [(C_0 - C_e)/m] \times V$, where m and V denote the mass of the sample and volume of Congo red solution respectively.

Aerosol particulate filtration efficiency of (coated) woven fabric

Aerosol particulate filtration efficiency was evaluated using an in-house built open circuit wind tunnel with a circular test

section of 70 mm in diameter. The inlet of the wind tunnel has a diameter of 200 mm and the converging duct has a contraction ratio of 8.16. The diffuser outlet has a diameter of 120 mm. A variable speed fan (DC axial fan, 270 $m^3\ h^{-1}$, 63.4 W, Sanyo Denki, Japan) is fitted at the exit of the diffuser to draw the aerosol through the sample. Aerosolised NaCl particles were used as the challenge particles and they were generated using a TSI particle generator (Model 8026 TSI Incorporated, Minnesota, USA) from a reservoir of 10 g L^{-1} NaCl solution. The face velocity upstream was 0.20 ± 0.05 m s^{-1}. The concentration of the NaCl particles upstream (C_u) and downstream (C_d) of the (coated) woven fabric was measured using a laser photometer (DustTrak II 8532, TSI Incorporated, Minnesota, USA) and the particulate filtration efficiency (η) of the (coated) woven fabric was calculated using: $\eta,\% = (1 - C_d/C_u) \times 100$. The measurement was triplicated and the average is reported for each sample.

Air permeability of (coated) woven fabric

Air permeability was quantified in accordance with ASTM D737-96 using an automated air permeability tester (Akustron, Rycobel Group, Flanders, Belgium) conducted at a differential pressure of 200 Pa over a sample with a test area of 26 cm^2.

Water vapour transmission rate of (coated) woven fabric

Water vapour transmission rate (WVTR) was determined in accordance with BS 7209:1990 under a controlled relative humidity (65 ± 2%) and temperature (20 ± 2 °C). Circular samples with a diameter of 83 mm were used. All samples were pre-conditioned for 5 h in this environment prior to WVTR measurements. A reference polyester woven fabric (mesh aperture = 18 mm, yarn diameter = 32 mm, number of threads = 196.1 cm^{-1}, open area = 12.5%) was tested concurrently alongside the (coated) woven fabrics as stipulated in the test standard for indexation. The measurement was triplicated and the average is reported for each sample.

Results and discussions

SEM revealed that the ZIF-67 particles synthesised in this work possessed a well-defined rhombic shape with smooth faces (see Fig. 1a). The average diameter of these ZIF-67 particles was found to be 440 ± 80 nm. When ZIF-67 was synthesised in the presence of BC, the ZIF-67 particles can be seen decorated onto the BC nanofibrils (see Fig. 1b). The average diameter of the ZIF-67 particles decorated onto the BC nanofibrils was also found to be 440 nm, implying that the presence of BC did not affect the crystal growth of ZIF-67 from solution. The weight fraction of ZIF-67 in ZIF-BC (w_{ZIF-67}) was quantified using TGA and a loading of 62 ± 4 wt% was estimated by comparing the residual mass at 700 °C (Fig. S1, ESI†). The composition and crystallographic structure of BC, ZIF-67 and ZIF-BC was confirmed with XRD (Fig. S2, ESI†). The XRD pattern of ZIF-BC has diffraction peaks originating from both BC and ZIF-67, suggesting that there are no changes to the crystallographic properties of ZIF-67 particles when grown in the presence of BC. FT-IR further showed that the ZIF-BC spectrum contained the all the characteristic peaks of both ZIF-67 and BC with no new absorbance peaks appearing (Fig. S3, ESI†). This suggests the ZIF-67 particles grew around the BC nanofibrils instead of forming a covalent bond with each other. It is however worth mentioning that the ZIF-67 particles were robustly attached onto the BC nanofibrils as we did not observe the detachment of ZIF-67 particles during the blending of ZIF-BC in water.

Fig. 2a presents the volumetric N_2 adsorption–desorption isotherms of ZIF-67, neat BC and ZIF-BC determined at −196 °C. It can be seen from this figure that BC exhibited a type II isotherm, accompanied by a type H3 hysteresis loop between $0.70 < P/P_0 < 0.99$. The observed reversible type II isotherm at $P/P_0 \leq 0.7$ is typical for material whereby the adsorption of N_2 molecules is unrestricted. The type H3 hysteresis loop at $P/P_0 > 0.7$ is indicative of BC behaving as non-rigid aggregates.[20] ZIF-67, on the other hand, exhibited a reversible type I isotherm, characteristic of a microporous solid with relatively small external surface area.[21] Such microporous solids have a steep uptake at very low P/P_0 (for ZIF-67, this occurred at $P/P_0 \leq 0.02$), followed by a plateau due to the amount of N_2 adsorbed approached the

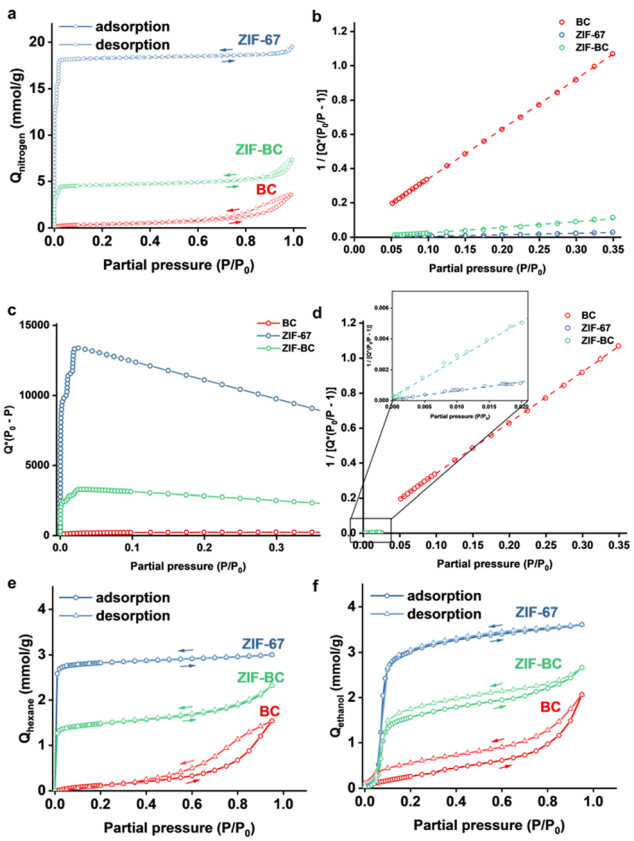

Fig. 2 N_2 adsorption–desorption and dynamic vapour adsorption analysis of BC (red), ZIF-BC (blue) and ZIF-BC (green). (a) N_2 adsorption–desorption isotherms, (b) BET plots computed using the standard P/P_0 range, (c) $Q(P/P_0)$ *vs.* P/P_0 plots to identify the valid P/P_0 range for subsequent BET analysis that satisfies the conditions outlined, (d) BET plots computed using the adjusted P/P_0 range, (e) dynamic *n*-hexane and (f) ethanol adsorption–desorption isotherms. Q = quantity sorbed.

limiting value (*i.e.*, all the accessible micropores had been filled). The sharp "knee" at $P/P_0 = 0.02$ confirms that the ZIF-67 particles possessed mainly narrow micropores of <1 nm[20] and this is in good agreement with the molecular structure of ZIF-67, which has a pore opening of 0.34 nm.[22] ZIF-BC exhibited a N_2 adsorption–desorption isotherm that combined both the adsorption–desorption behaviour of ZIF-67 and BC; a steep N_2 uptake at low P/P_0 followed by a plateau (characteristic of ZIF-67) and a type H3 hysteresis at $0.80 < P/P_0 < 0.99$ (characteristic of BC). These results indicate that the micropores of the ZIF-67 particles decorated on ZIF-BC are still accessible. The BET plots ($1/Q(P_0/P - 1)$ *vs.* P/P_0) of ZIF-67, BC and ZIF-BC are presented in Fig. 2b. By default, BET analysis to determine the specific surface area of a material is performed over the range of $0.05 < P/P_0 < 0.35$.[23] Whilst this BET range is generally applicable to most materials, it has been shown that this P/P_0 range is not suitable for MOFs due to its unique pore structure.[24]

The use of this default BET range for the specific surface area determination of BC should also be verified.[25] The BET surface area calculated from this default P/P_0 range is tabulated in Table 1. Whilst a positive BET surface area was obtained, the *c*-value, which corresponds to the enthalpy of adsorption, was found to be negative for both ZIF-67 and ZIF-BC. This is because BET analysis assumes that adsorption occurs by multilayer formation and that there is no steric limitation to the thickness of the multilayer at the saturation pressure, *i.e.* adsorption occurs as if it was on a free surface.[25] These assumptions do not hold for MOFs, whereby the adsorption is dominated by a pore-filling mechanism.[26] In addition to this, the micropores in ZIF-67 are completely filled with N_2 molecules at pressure well below the BET range (as illustrated in Fig. 2a).

To account for these effects, three selection criteria as outlined by Rouquerol *et al.*[24,25] were further used to choose an appropriate P/P_0 range for our BET analysis: (i) the *y*-intercept of the BET plot must be positive to obtain a positive *c*-value in the selected P/P_0 range, (ii) the calculated monolayer capacity (Q_m) must lie within the selected P/P_0 range and (iii) $Q(P_0 - P)$ must increase with increasing P/P_0. A plot of $Q(P_0 - P)$ *vs.* P/P_0 for ZIF-67, BC and ZIF-BC is presented in Fig. 2c. It can be seen from this figure that $Q(P_0 - P)$ of BC increased with P/P_0 (over the standard BET range). For both ZIF-67 and ZIF-BC however, $Q(P_0 - P)$ increased with P/P_0 only up to $P/P_0 = 0.025$ and $P/P_0 = 0.022$, respectively. Therefore, only the first few data points should be included in the subsequent BET analysis (see Fig. 2d for the BET plots with an adjusted P/P_0 range). Based on this, a specific surface area (A_s) of $\sim$1750 $m^2\ g^{-1}$ was obtained for ZIF-67 (see Table 1), which is similar to those reported in the literature.[27,28] Due to the presence of ZIF-67, the A_s of ZIF-BC was found to be $\sim$410 $m^2\ g^{-1}$, 1100% increase over neat BC.

The vapour sorption behaviour of a material is also important, particularly for protective suit applications. In this work, *n*-hexane and ethanol were used as representative non-polar and polar probe molecules, respectively, to characterise the vapour sorption of BC, ZIF-67 and ZIF-BC at 25 °C for use as a vapour adsorbing coating for a fabric substrate. The *n*-hexane adsorption isotherms for these 3 different materials are shown in Fig. 2e. These isotherms followed a similar trend as the volumetric N_2 adsorption isotherms. *n*-Hexane adsorption by ZIF-67 is best described by a type I isotherm. At a concentration as low as $P/P_0 = 0.01$, ZIF-67 was found to adsorb 2.6 mmol g^{-1} of *n*-hexane, comparable to typical industrial adsorbents such as activated charcoal at the same P/P_0 (2.3 mmol g^{-1}).[29] The *n*-hexane adsorption on BC is of a type II isotherm and the maximum *n*-hexane uptake of neat BC at $P/P_0 = 0.9$ was 1.4 mmol g^{-1}. Such low *n*-hexane uptake can be attributed to the low specific surface area, as well as the hydrophilic properties of BC, which has a measured water-in-air contact angle of $\sim 20°$.[30] For ZIF-BC, the *n*-hexane adsorption isotherm is characterised by a steep uptake at low P/P_0 of up to $P/P_0 = 0.1$, followed by a typical type II isotherm between $0.1 < P/P_0 < 0.9$. The amount of *n*-hexane adsorbed at $P/P_0 = 0.01$ was found to be 1.3 mmol g^{-1}. This corroborates with the $w_{ZIF\text{-}67}$ of ZIF-BC and is comparable to that of zeolite Y at the same P/P_0 (1.0 mmol g^{-1}).[29] Such adsorption isotherm suggests that it is more favourable for *n*-hexane to adsorb by first filling the micropores of ZIF-67 particles before adsorbing onto the BC surface. The adsorption isotherm of ethanol (Fig. 2f) for both ZIF-67 and ZIF-BC appeared to be different compared to their respective *n*-hexane adsorption isotherms. Both ZIF-67 and ZIF-BC exhibited poor ethanol uptake at $P/P_0 < 0.05$. Cage-filling only occurred after this P/P_0. This inflection had been observed previously when alcohol molecules were adsorbed onto hydrophobic zeolites.[31] This can be attributed to the difficulties in overcoming the electrostatic barrier of the pores by polar molecules and the hydrophobicity of ZIFs. The maximum ethanol adsorbed by ZIF-67 and ZIF-BC was found to be 3.6 mmol g^{-1} and 2.4 mmol g^{-1}, respectively: 40% lower than their respective *n*-hexane adsorption. Ethanol adsorption on neat BC still resembled a type II isotherm and the maximum uptake at $P/P_0 = 0.9$ was higher than that of *n*-hexane at 1.7 mmol g^{-1}, presumably due to the presence of large amount of hydroxyl groups on BC.

The sorption of liquid CWAs is also vital to maximise dermal protection provided by a protective suit if the shell fabric is no longer oleophobic and hydrophobic. Here, Congo red was used as the representative dye to simulate the sorption of liquid

Table 1 Surface area (A_s) from N2 adsorption calculated with the standard BET range of $0.05 < P/P_0 < 0.35$ (standard) and with the P/P_0 range determined with Fig. 2c (adjusted)

	Standard BET range			Adjusted BET range			
Sample	A_s ($m^2\ g^{-1}$)	Q_m (mmol g^{-1})	*c*-value	P/P_0 range	A_s ($m^2\ g^{-1}$)	Q_m (mmol g^{-1})	*c*-value
BC	33 ± 1	0.3 ± 0.1	59 ± 1	0.05–0.35	33 ± 1	0.3 ± 0.1	59 ± 1
ZIF-67	1169 ± 30	12.0 ± 0.3	−33 ± 6	0.001–0.025	1747 ± 50	17.9 ± 0.5	599 ± 100
ZIF-BC	302 ± 6	3.1 ± 0.1	−41 ± 6	0.001–0.022	411 ± 10	4.2 ± 0.1	660 ± 200

Table 2 Fitting parameters of Congo red sorption from the liquid phase

	Langmuir			Freundlich		
Sample	Q_{max} (mg g^{-1})	K_L	R^2	K_F (mg g^{-1})(L g^{-1})$^{-1/n}$	n	R^2
BC	19 ± 4	0.04 ± 0.01	0.871	0.7 ± 0.1	1.1 ± 0.1	0.993
ZIF-67	526 ± 80	0.05 ± 0.01	0.906	37.8 ± 8.0	1.6 ± 0.2	0.924
ZIF-BC	210 ± 20	0.10 ± 0.02	0.946	34.9 ± 4.0	2.2 ± 0.2	0.957
Cotton	3 ± 1	0.14 ± 0.06	0.959	0.2 ± 0.1	1.2 ± 0.1	0.964
ZIF-cotton	26 ± 8	0.06 ± 0.02	0.768	5.0 ± 0.6	3.3 ± 0.6	0.898
ZIF-BC on cotton at 0.25 g m^{-2}	8 ± 1	0.06 ± 0.01	0.925	0.4 ± 0.1	1.2 ± 0.1	0.958
ZIF-BC on cotton at 0.5 g m^{-2}	10 ± 1	0.04 ± 0.01	0.946	0.6 ± 0.1	1.5 ± 0.1	0.999
ZIF-BC on cotton at 1 g m^{-2}	10 ± 1	0.18 ± 0.06	0.932	1.6 ± 0.2	1.6 ± 0.2	0.958

CWAs. The equilibrium experimental data were fitted with the linearised Langmuir and Freundlich model (Fig. S4 and S5, ESI†) and the fitting parameters are tabulated in Table 2. The R^2 of the Freundlich model was found to be higher than the R^2 of the Langmuir model, a result which suggests that non-uniform multilayer Congo red adsorption has taken place.[32,33] Focussing on the Freundlich model, the term K_F corresponds to the adsorption capacity, whilst the term $1/n$ denotes the adsorption intensity or surface heterogeneity and provides an indication whether the adsorption is a favourable one. Based on the Freundlich model, ZIF-67 had the highest Congo red adsorption capacity of 37 (mg g^{-1})(L g^{-1})$^{-1/n}$, followed by ZIF-BC at 35 (mg g^{-1})(L g^{-1})$^{-1/n}$ and BC at 1 (mg g^{-1})(L g^{-1})$^{-1/n}$, closely tracking the A_s of these materials (Table 1). The value of $1/n$ was observed to be <1 across all samples, indicates that Congo red adsorption in these materials is favourable.[34] It is also worth highlighting that the reported K_F values for ZIF-67 and ZIF-BC are notably higher than that of laboratory grade activated carbon (1 (mg g^{-1})(L g^{-1})$^{-1/n}$)[35] and zeolite (28 (mg g^{-1})(L g^{-1})$^{-1/n}$),[36] suggesting the strong adsorption capacity of the synthesised ZIF-67 and ZIF-BC.

It is evident that the liquid and vapor sorption of BC is enhanced with ZIF-67 decoration. We then investigated its performance as a coating for protective suit by coating the ZIF-BC onto a plain weave woven cotton fabric using a papermaking process. Different BC grammages were investigated (0.25 g m^{-2}, 0.5 g m^{-2} and 1 g m^{-2}). As a control, ZIF-67 decorated plain weave woven fabric (ZIF-cotton) was also prepared following a similar protocol to prepare ZIF-BC. The ZIF-67 loading in the ZIF-cotton was determined to be ~4 wt% based on simple weight gain measurements.

Uncoated woven fabric (Fig. 3a) has an aperture, *i.e.*, distance between adjacent yarns, of ~70 μm. ZIF-cotton (Fig. 3b) also took the purple colour of ZIF-67 and still possessed a similar open structure, albeit with ZIF-67 particles densely packed on the surface of the cotton yarns. The coverage of the ZIF-BC on woven fabric using 1-filtration and 2-filtration strategies is presented in Fig. 3c and d, respectively. As expected, increasing BC grammage in the ZIF-BC coating increases its coverage on the woven fabric and the coverage achieved by 2-filtration is better than 1-filtration. This can be attributed to the partial blocking of the pores on the woven fabric in the first vacuum filtration step. The ZIF-BC in water suspension in the second vacuum filtration step can only flow through the uncoated regions of the woven fabric, *i.e.*, flow through the path of least resistance, increasing the ZIF-BC coverage. Full coverage of the woven fabric by ZIF-BC can be achieved at a BC grammage of 1 g m^{-2} using 2-filtration.

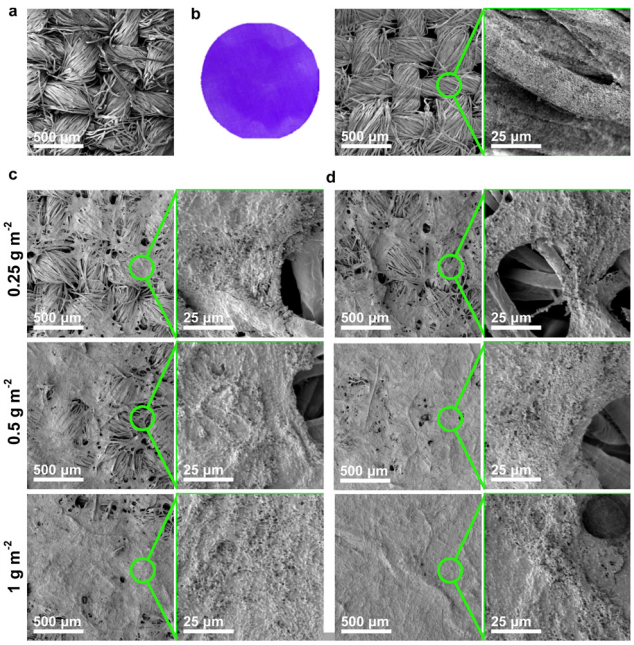

Fig. 3 SEM images showing the morphology of (a) uncoated woven fabric, (b) ZIF-cotton, as well as ZIF-BC coated woven fabric using (c) 1-filtration and (d) 2-filtration.

The air permeability, aerosol particulate filtration performance and water vapour transmission rate (WVTR) of the uncoated woven fabric, ZIF-cotton and ZIF-BC coated woven fabric are also evaluated. Without any coating, the woven fabric was found to possess an air permeability of ~600 mm s^{-1} (Fig. 4a). The decoration of ZIF-67 on the woven fabric (ZIF-cotton) led to a 30% decrease in air permeability to ~420 mm s^{-1}. It can also be seen that increasing the grammage of ZIF-BC coating leads to a decrease in air permeability. At a grammage of 0.25 g m^{-2}, the ZIF-BC coated woven fabric manufactured using 1-filtration was found to possess an air permeability of 250 mm s^{-1}. Increasing the coating grammage to 1 g m^{-2} reduced the air permeability by a factor of 15 to *ca.* 17 mm s^{-1}. With 2-filtration, the air permeability of ZIF-BC coated woven fabric decreased to 130 mm s^{-1} and 11 mm s^{-1}, respectively. This is due to the blocking of the flow channels in between the yarns with the ZIF-BC coating.

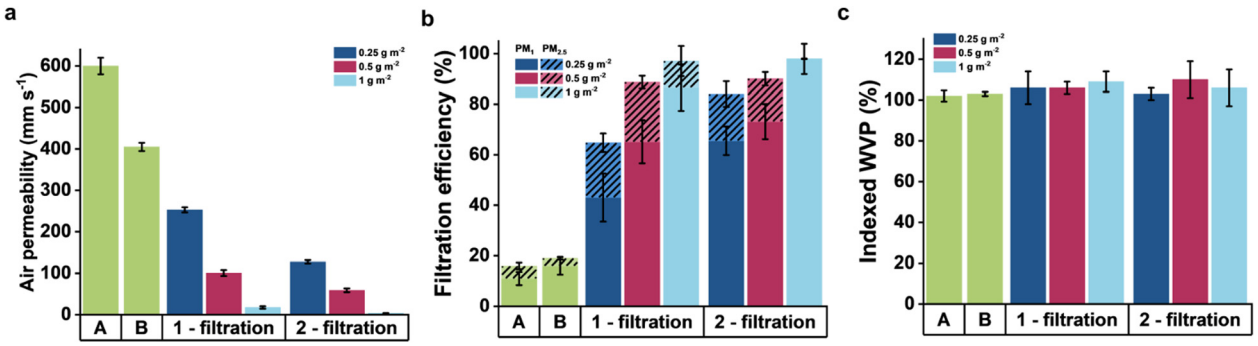

Fig. 4 (a) Air permeability, (b) aerosol particulate filtration efficiency and (c) indexed water vapour transmission rate of uncoated woven fabric (A), ZIF-cotton (B) and ZIF-BC coated woven fabric fabricated with the single filtration strategy (1-filtration) and double filtration strategy (2-filtration), while PM_1 and $PM_{2.5}$ denote particulate matter with size less than 1 and 2.5 μm respectively.

The aerosol particulate filtration performance of the ZIF-BC woven fabrics is presented in Fig. 4b. All ZIF-BC coated woven fabrics possess enhanced aerosol particulate filtration performance compared to uncoated and only ZIF-coated woven fabric (ZIF-cotton), which has a similar aerosol particulate filtration efficiency of ~16%. This similarity is also indicative that aerosol particulate filtration performance is not only governed by air permeability (as ZIF-cotton has lower air permeability than uncoated woven fabric) but by the pore opening between the yarns (which is similar between the two samples). The aerosol particulate filtration efficiency increased to 97% for PM_1 and 98% for $PM_{2.5}$ by just coating 1 g m^{-2} of ZIF-BC. This is because the opening between the yarns have been blocked by the coating and thus, more aerosolised NaCl particles are now rejected by a size exclusion mechanism. It is worth mentioning at this point that the air permeability and the aerosol particulate filtration efficiency of the ultra-low grammage ZIF-BC coated woven fabrics are similar to that of neat BC-coated woven fabrics.[37]

ZIF-67 is hydrophobic, with an estimated advancing water contact angle of ~120°.[38] Couple this with the reduced air permeability, the coating of ZIF-BC may lead to a significant reduction in WVTR. This will then result in heat stress[17] if ZIF-BC is used as a coating for the shell fabric of a protective suit. Nonetheless, WVTR measurement showed otherwise (Fig. 4c). The WVTR of all the samples was found to be similar, suggesting that addition of a hydrophobic ZIF-67 would not impede moisture permeance. This could be attributed to the low loading of ZIF-67 in the resultant coated woven fabric.

The adsorption of Congo red from the aqueous phase by ZIF-cotton and ZIF-BC coated woven fabrics was also investigated and the respective Freundlich constants (K_F and n) are presented in Table 2. The adsorption of Congo red on these samples is also favourable as indicated by $1/n < 1$. The K_F of these samples scale with the amount of ZIF loading (ZIF-cotton > 1 g m^{-2} ZIF-BC coated woven fabric > 0.5 g m^{-2} ZIF-BC coated woven fabric > 0.25 g m^{-2} ZIF-BC coated woven fabric).

Conclusions

In this work, we have successfully demonstrated a simple and scalable method to decorate BC with ZIF-67 for use as a multi-functional coating to enhance the barrier properties of woven textiles. The growth of ZIF-67 from solution was not affected by the presence of BC and the attachment of ZIF-67 onto BC was found to be robust. With the decoration of ZIF-67 onto BC, an increase in specific surface area, liquid and vapour sorption capacity is shown with ZIF-BC when compared with neat BC. As a textile coating, an aerosol particulate filtration efficiency of 66% for PM_1 and 83% for $PM_{2.5}$ was achieved at a grammage of 0.25 g m^{-2}. Increasing the coating grammage to 1 g m^{-2} increased the aerosol particulate filtration efficiency to 97% for PM_1 and 98% for $PM_{2.5}$. Such increase is attributed to the blocking of the pores by the ZIF-67 decorated BC coating, which rejects the aerosolised particulates by a size exclusion mechanism. This cannot be achieved with just ZIF-67 grown onto the woven textile without BC, which possessed an aerosol filtration efficiency of only 16% and 19% for PM_1 and $PM_{2.5}$, respectively. The ZIF-67 decorated BC coating also did not affect the moisture permeability of the woven textile.

Data availability

The data supporting this article has been included as part of the ESI.†

Conflicts of interest

There are no conflicts to declare.

Acknowledgements

This work is supported by the UK Defence Science and Laboratory (dstl) (contract number: DSTL-1000144773). We also greatly appreciate the funding provided by Imperial College London Open Access Fund for making this article open access.

Notes and references

1 M. P. Krafft and J. G. Riess, Per- and polyfluorinated substances (PFASs): Environmental challenges, *Curr. Opin. Colloid Interface Sci.*, 2015, **20**, 192–212.

2 H. S. Jhinjer, A. Singh, S. Bhattacharya, M. Jassal and A. K. Agrawal, Metal-organic frameworks functionalized smart textiles for adsorptive removal of hazardous aromatic pollutants from ambient air, *J. Hazard. Mater.*, 2021, **411**, 125056.
3 S. Guo, P. Zhang, Y. Feng, Z. Wang, X. Li and J. Yao, Rational design of interlaced Co9S8/carbon composites from ZIF-67/cellulose nanofibers for enhanced lithium storage, *J. Alloys Compd.*, 2020, **818**, 152911.
4 S. Saeed, R. Bashir, S. U. Rehman, M. T. Nazir, Z. A. ALOthman, A. Muteb Aljuwayid, A. Abid and A. Adnan, Synthesis and Characterization of ZIF-67 Mixed Matrix Nanobiocatalysis for CO2 Adsorption Performance, *Front. Bioeng. Biotechnol.*, 2022, **10**, 891549.
5 W. Sun, X. Zhai and L. Zhao, Synthesis of ZIF-8 and ZIF-67 nanocrystals with well-controllable size distribution through reverse microemulsions, *Chem. Eng. J.*, 2016, **289**, 59–64.
6 J. Park and M. Oh, Construction of flexible metal–organic framework (MOF) papers through MOF growth on filter paper and their selective dye capture, *Nanoscale*, 2017, **9**, 12850–12854.
7 M. Jahan, Q. Bao and K. P. Loh, Electrocatalytically Active Graphene–Porphyrin MOF Composite for Oxygen Reduction Reaction, *J. Am. Chem. Soc.*, 2012, **134**, 6707–6713.
8 J.-L. Zhuang, D. Ar, X.-J. Yu, J.-X. Liu and A. Terfort, Patterned Deposition of Metal-Organic Frameworks onto Plastic, Paper, and Textile Substrates by Inkjet Printing of a Precursor Solution, *Adv. Mater.*, 2013, **25**, 4631–4635.
9 S. Ma, M. Zhang, J. Nie, J. Tan, S. Song and Y. Luo, Lightweight and porous cellulose-based foams with high loadings of zeolitic imidazolate frameworks-8 for adsorption applications, *Carbohydr. Polym.*, 2019, **208**, 328–335.
10 Y. Wu, W. Ren, Y. Li, J. Gao, X. Yang and J. Yao, Zeolitic Imidazolate Framework-67@Cellulose aerogel for rapid and efficient degradation of organic pollutants, *J. Solid State Chem.*, 2020, **291**, 121621.
11 Q. Zhang, Y. Cheng, C. Fang, J. Shi, J. Chen and H. Han, Functionalized waste cellulose with metal-organic-frameworks as the adsorbent with adjustable pore size: Ultralight, effective, and selective removal of organic dyes, *J. Solid State Chem.*, 2021, **302**, 122361.
12 T. Mai, P.-L. Wang, Q. Yuan, C. Ma and M.-G. Ma, In situ anchoring Zn-doped ZIF-67 on carboxymethylated bacterial cellulose for effective indigo carmine capture, *Nanoscale*, 2021, **13**, 18210–18217.
13 L. Zhu, L. Zong, X. Wu, M. Li, H. Wang, J. You and C. Li, Shapeable Fibrous Aerogels of Metal–Organic-Frameworks Templated with Nanocellulose for Rapid and Large-Capacity Adsorption, *ACS Nano*, 2018, **12**, 4462–4468.
14 K. Zhang, W. Hutcherson, N. D. Evans, T. Elder, C. M. Garner and M. Li, In situ synthesis of metal-organic frameworks on sulfonated cellulose nanofibrils, *Solid State Sci.*, 2024, **158**, 107755.
15 FutureMarkets, The global market for cellulose nanofibers to 2031, **https://www.futuremarketsinc.com/the-global-market-for-cellulose-nanofibers-to-2031**.
16 J. Li, T. Tammelin, C. Stone, M. Dennis and K.-Y. Lee, Ultra-Low Grammage Nanocellulose-Coated Woven Fabric with Improved Aerosol Particulate Filtration Performance, *Adv. Mater. Interfaces*, 2024, **11**, 2400424.
17 K. K. Kraning and R. R. Gonzalez, Physiological consequences of intermittent exercise during compensable and uncompensable heat stress, *J. Appl. Physiol.*, 1991, **71**, 2138–2145.
18 A. Santmarti, J. W. Teh and K.-Y. Lee, Transparent Poly(methyl methacrylate) Composites Based on Bacterial Cellulose Nanofiber Networks with Improved Fracture Resistance and Impact Strength, *ACS Omega*, 2019, **4**, 9896–9903.
19 S. A. Han, J. Lee, K. Shim, J. Lin, M. Shahabuddin, J.-W. Lee, S.-W. Kim, M.-S. Park and J. H. Kim, Strategically Designed Zeolitic Imidazolate Frameworks for Controlling the Degree of Graphitization, *Bull. Chem. Soc. Jpn.*, 2018, **91**, 1474–1480.
20 M. Thommes, K. Kaneko, A. V. Neimark, J. P. Olivier, F. Rodriguez-Reinoso, J. Rouquerol and K. S. W. Sing, Physisorption of gases, with special reference to the evaluation of surface area and pore size distribution (IUPAC Technical Report), *Pure Appl. Chem.*, 2015, **87**, 1051–1069.
21 L. M. Anovitz and D. R. Cole, Characterization and Analysis of Porosity and Pore Structures, *Rev. Mineral. Geochem.*, 2015, **80**, 61–164.
22 Z. Pouramini, S. M. Mousavi, A. Babapoor, S. A. Hashemi, C. W. Lai, Y. Mazaheri and W.-H. Chiang, Effect of Metal Atom in Zeolitic Imidazolate Frameworks (ZIF-8 & 67) for Removal of Dyes and Antibiotics from Wastewater: A Review, *Catalysts*, 2023, **13**, 155.
23 S. Brunauer, P. H. Emmett and E. Teller, Adsorption of Gases in Multimolecular Layers, *J. Am. Chem. Soc.*, 1938, **60**, 309–319.
24 J. Rouquerol, P. Llewellyn and F. Rouquerol, in *Studies in Surface Science and Catalysis*, ed. P. L. Llewellyn, F. Rodriquez-Reinoso, J. Rouqerol and N. Seaton, Elsevier, 2007, vol. 160, pp. 49–56.
25 A. Kondor, A. Santmarti, A. Mautner, D. Williams, A. Bismarck and K.-Y. Lee, On the BET Surface Area of Nanocellulose Determined Using Volumetric, Gravimetric and Chromatographic Adsorption Methods, *Front. Chem. Eng.*, 2021, **3**, 738995.
26 J. L. C. Rowsell and O. M. Yaghi, Effects of Functionalization, Catenation, and Variation of the Metal Oxide and Organic Linking Units on the Low-Pressure Hydrogen Adsorption Properties of Metal−Organic Frameworks, *J. Am. Chem. Soc.*, 2006, **128**, 1304–1315.
27 W. Li, A. Zhang, X. Jiang, C. Chen, Z. Liu, C. Song and X. Guo, Low Temperature CO2 Methanation: ZIF-67-Derived Co-Based Porous Carbon Catalysts with Controlled Crystal Morphology and Size, *ACS Sustainable Chem. Eng.*, 2017, **5**, 7824–7831.
28 N. Hammi, N. Couzon, T. Loiseau, C. Volkringer, A. El Kadib, S. Royer and J. Dhainaut, Hierarchically porous ZIF-67/chitosan beads with high surface area and strengthened mechanical properties: Application to CO2 storage, *Mater. Today Sustainability*, 2023, **22**, 100394.
29 E. Hunter-Sellars, J. J. Tee, I. P. Parkin and D. R. Williams, Adsorption of volatile organic compounds by industrial porous materials: Impact of relative humidity, *Microporous Mesoporous Mater.*, 2020, **298**, 110090.
30 M. S. Peresin, K. Kammiovirta, H. Heikkinen, L.-S. Johansson, J. Vartiainen, H. Setälä, M. Österberg and T. Tammelin, Understanding the mechanisms of oxygen diffusion through surface

functionalized nanocellulose films, *Carbohydr. Polym.*, 2017, **174**, 309–317.
31 I. Halasz, S. Kim and B. Marcus, Uncommon Adsorption Isotherm of Methanol on a Hydrophobic Y-zeolite, *J. Phys. Chem. B*, 2001, **105**, 10788–10796.
32 K. Y. Foo and B. H. Hameed, Insights into the modeling of adsorption isotherm systems, *Chem. Eng. J.*, 2010, **156**, 2–10.
33 S. Kalam, S. A. Abu-Khamsin, M. S. Kamal and S. Patil, Surfactant Adsorption Isotherms: A Review, *ACS Omega*, 2021, **6**, 32342–32348.
34 T. Santhi, S. Manonmani, T. Smitha, D. Sugirtha and K. Mahalakshmi, Uptake of Cationic Dyes from Aqueous Solution by Bioadsorption onto Granular Cucumis Sativa, *J. Appl. Sci. Environ. Sanit.*, 2009, **4**, 927406.
35 I. D. Mall, V. C. Srivastava, N. K. Agarwal and I. M. Mishra, Removal of congo red from aqueous solution by bagasse fly ash and activated carbon: Kinetic study and equilibrium isotherm analyses, *Chemosphere*, 2005, **61**, 492–501.
36 R. Nodehi, H. Shayesteh and A. R. Kelishami, Enhanced adsorption of congo red using cationic surfactant functionalized zeolite particles, *Microchem. J.*, 2020, **153**, 104281.
37 J. Li, T. Tammelin, C. Stone, M. Dennis and K.-Y. Lee, Ultra-Low Grammage Nanocellulose-Coated Woven Fabric with Improved Aerosol Particulate Filtration Performance, *Adv. Mater. Interfaces*, 2024, 2400424.
38 E. Hunter-Sellars, P. A. Saenz-Cavazos, A. R. Houghton, S. R. McIntyre, I. P. Parkin and D. R. Williams, Sol–Gel Synthesis of High-Density Zeolitic Imidazolate Framework Monoliths via Ligand Assisted Methods: Exceptional Porosity, Hydrophobicity, and Applications in Vapor Adsorption, *Adv. Funct. Mater.*, 2021, **31**, 2008357.